frontiers | Frontiers in Materials

TYPE Original Research
PUBLISHED 06 June 2024
DOI 10.3389/fmats.2024.1420131

OPEN ACCESS

EDITED BY
Di Wang,
University of Ottawa, Canada

REVIEWED BY
Salvatore Verre,
University of eCampus, Italy
Fan Zhang,
Aalto University, Finland
Teng Wang,
University of Pisa, Italy

*CORRESPONDENCE
Xupeng Sun,
22107029@stu.sdjtu.edu.cn

RECEIVED 19 April 2024
ACCEPTED 13 May 2024
PUBLISHED 06 June 2024

CITATION
Zhang Y, Peng G, Li A, Yang X, Kong S, An Y, Tian J and Sun X (2024), Research on the resistance of cement-based materials to sulfate attack based on MICP technology. *Front. Mater.* 11:1420131. doi: 10.3389/fmats.2024.1420131

Research on the resistance of cement-based materials to sulfate attack based on MICP technology

Yong Zhang[1], Geng Peng[2,3], Ai Li[1], Xinrui Yang[2,3], Shuaidi Kong[1], Yutong An[4], Junhao Tian[4] and Xupeng Sun[4]*

[1]Beijing Capital International Airport Co., Beijing, China, [2]Beijing Municipal Engineering Research Institute, Beijing, China, [3]Beijing Municipal Road and Bridge Technology Development Co., Beijing, China, [4]School of Transportation Civil Engineering, Shandong Jiaotong University, Jinan, China

To evaluate the effect of Microbial Induced Calcium Carbonate Precipitation (MICP) on the enhancement of early resistance to sulfate attack of cementitious materials. In this paper, firstly, the effect of *Bacillus subtilis* (BM) on the carbonation depth as well as the carbonation rate of standard as well as carbonation-conditioned cementitious sand specimens was investigated. Secondly, the compressive strength and volumetric deformation of the specimens at different ages of immersion in sulfate solution were investigated. Finally, the changes of hydration products before and after the addition of BM were analyzed by X-ray diffraction analysis (XRD), and the microscopic pore structure of the specimens after erosion was analyzed by low-field nuclear magnetic resonance (LF-NMR) and scanning electron microscope (SEM), which revealed the mechanism of the improvement of BM on the resistance to sulfate erosion of the cementitious materials. The results showed that the initial compressive strength of BM carbonised curing specimens, ordinary carbonised curing specimens and BM standard curing specimens were increased by 42.0%, 34.0% and 4.0%, respectively, compared with the ordinary standard curing specimens, respectively, compared with the control group, and the loss of the final compressive strength was reduced by 37.4%, 25.4%, and 14.5%, and the expansion rate was reduced by 31.3%, 22.0%, after sulfate erosion for 6 months, 5.2%, and porosity decreased by 24.2%, 13.6%, and 9.9%. Microbial mineralization accelerated the reaction between Ca^{2+} in the pore solution and atmospheric CO_2, and the calcite formed filled the pores to make the structure denser, increasing the initial compressive strength of the specimens and reducing the loss of properties when exposed to sulfate solution. Therefore, the application of MICP technology in cementitious materials provides a new direction for the development of durable and sustainable cementitious materials.

KEYWORDS

microbial mineralisation, CO_2 conservation, sulfate erosion, cementitious materials, microstructure

1 Introduction

Complex environmental factors (e.g., temperature, humidity, aggressive ions, etc.) during concrete service can have an impact on concrete durability (Yin et al., 2019; Li and Gan, 2023), among which sulfate attack is an important influence on concrete durability (Zhang et al., 2021a). This is mainly due to the diffusion of sulfate ions (SO_4^{2-}) into the concrete by combining with magnesium (Mg^{2+}), sodium (Na^+) and potassium (K^+) ions, which can react with calcium hydroxide (CH) and alumina to form gypsum ($CaSO_4$-$2H_2O$), magnesium hydroxide ($Mg(OH)_2$), and hydrate Sulphate Aluminate of Calcium (AFt) (Santhanam et al., 2003; Wu et al., 2024a; Wu et al., 2024b). These chemical changes disrupt the original chemical equilibrium in the hydrated cement system, which in turn triggers the swelling of the material as well as the deterioration of the C-S-H gel, which may ultimately lead to cracking and inevitable structural degradation (Jiang et al., 2021). Therefore, it is crucial to adopt effective methods to improve the resistance of cementitious materials to sulphate attack in.

By placing cementitious materials at the early stage of hydration in a high concentration of carbon dioxide, carbonation maintenance can make cement clinker minerals such as tricalcium silicate (C_3S) and dicalcium silicate (C_2S) and hydration products such as calcium hydroxide (CH) and hydrated calcium silicate (C-S-H) undergo a carbonation reaction at the same time, to make the cement slurry have a higher strength within a short period, and to improve the performance of cementitious materials effectively. (Zhang et al., 2017; Wu et al., 2021; Xu et al., 2024). In recent years, this technology has been widely used in block maintenance (Meng et al., 2019), freeze-thaw resistance (Ding et al., 2022), resistance to dissolution damage (Zhang et al., 2021b), recycled aggregate reinforcement (Ahmad et al., 2023), and enhancing the performance of reinforced concrete as well as fibre concrete, etc., (Salvatore, 2021; Xian et al., 2022). Seo et al. (Seo et al., 2018) investigated the long-term performance of the carbonation-conditioned cement mortar in an acidic aggressive environment, and the results showed that carbonation-conditioned cement mortar in a sulphuric acid-aggressive environment will generate calcium sulfate precipitation to replace calcium alumina, which will lead to the formation of calcium sulfate precipitate, and thus the carbonation-conditioned cement mortar will have a higher strength in a short period. Replace calcium alumina, thus enhancing the durability of cement screeds in acidic environments. Rostami et al. (2012)found that concrete that has undergone carbonation curing forms a dense, reinforced surface layer that reduces the amount of unstable, easily soluble calcium hydroxide in the hydration products, and thus improves the permeability, sulphate attack resistance and frost resistance of the concrete. Su et al. (2022) used carbonation-treated high-calcium fly ash as supplementary cementitious material to prepare cement mortar, to study the synergistic effect of carbonation treatment and carbonation curing on the improvement of specimen resistance to sulfate erosion, and found that the synergistic carbonation treatment and carbonation curing reduced the content of expansive free CaO, improved the pore structure of the specimen and reduced permeability; et al. (Qin et al., 2022) by combining the carbonation curing with gangue powder, and similarly achieved a better effect. To obtain a high carbonation rate, high specific surface area (Lily et al., 2019; Chen, 2020), pre-compression molding (Falchetto et al., 2018; Liang et al., 2020), elevated CO_2 concentration (Kashef-Haghighi et al., 2015), and pressurized curing (Dixit et al., 2021) are usually used, which have high technical and economic costs, and in a high concentration of CO_2, a protective film of $CaCO_3$ is formed on the surface of the specimen, which prevents internal carbonation (Polettini et al., 2016; Jia, 2020). The introduction of bacteria into cementitious materials has been considered an effective method to accelerate the carbonation process (Sha et al., 2020; Liang et al., 2022; Xing et al., 2023). It was found that carbonic anhydrase (CA) secreted by BM has the property of accelerating the hydration of CO_2 to HCO_3^-, and its secretion also has certain gelling properties, which can theoretically increase the rate of the hydration reaction by about 10^7-fold, and significantly enhance the efficiency and rate of CO_2 uptake (Rui and Qian, 2022). Zhang et al. (2022) investigated the effect of cement on the stability and strength of steel slag cementitious materials, and the results of the study showed that the incorporation of mineralizing bacteria into the steel slag cementitious materials could accelerate the rate of carbonation reaction of various mineral phases, and increase the degree of carbonation reaction, and the conversion of f-CaO to calcium carbonate increased the compressive strength of cementitious materials and reduced the linear expansion rate. Tayebani and Mostofinejad (2019) cured microbial concrete in a urea-calcium lactate mixture, and the specimens showed a reduction in water absorption and chloride permeability, and an increase in compressive strength, corrosion resistance, and electrical resistance. L et al. (Chaurasia et al., 2019) explored the effect of a new method of deposition that enhances both the macro and micro properties of concrete. Osman and Taher (2021) used microbial reinforced concrete made with *Bacillus* globulus and *Bacillus* pastures to show better corrosion resistance of reinforcing steel as compared to normal concrete, and the higher the concentration of the two microbial cells, the lower the maximum anodic current and the lower the corrosion rate. In addition, MICP technology has also achieved better results in the post-maintenance of common cementitious materials, Muynck et al. used an overlay to coat the mortar surface with microorganisms and nutrients to biomineralise the mortar surface, inducing the production of calcium carbonate, which resulted in a reduction of carbonation and chloride infiltration by 25%–30% and 10%–40%, respectively, and an enhanced resistance to freeze-thaw cycling. These studies verified the feasibility of MICP technology applied to cement concrete and pointed out the direction to regulate the microbial mineralization deposition process.

At present, many scholars have conducted a large number of experimental studies on microbial mineralisation technology to enhance the rate of cement carbonation, but there is still a relative lack of research on microbial mineralisation to enhance the sulphate erosion resistance of cementitious materials. Therefore, it is necessary to investigate the mechanical and durability properties of microbial mineralized cementitious materials after sulfate erosion. In this work, the anti-sulfate erosion properties of cementitious materials under stable pressure after microbial mineralization maintenance were investigated to study the effects of carbonation microorganisms as well as carbonation maintenance on the anti-sulfate erosion properties of cementitious materials. The microstructural changes and deterioration mechanism of cementitious materials after sulfate erosion were analyzed by XRD,

TABLE 1 Chemical composition of cement (%).

	CaO	SiO_2	Al_2O_3	Fe_2O_3	MgO	SO_3	Na_2O	LOL
Cement	67.72	22.13	4.54	2.36	2.73	2.61	0.13	2.78

LF-NMR, and SEM. The study can provide a certain experimental basis for the improvement of sulfate erosion resistance and durability of cementitious materials.

2 Materials and methods

2.1 Materials

2.1.1 Cement

P.II 42.5 cement produced in Shandong, China, with a specific surface area of 353.0 m^2/kg was used and the chemical composition is shown in Table 1.

2.1.2 Mineralised bacteria

The microorganism selected for this study was *Bacillus* Mucilaginosus (BM) as shown in Figure 1. This strain is highly alkaline environment adaptable and harmless to the human body and environment. The carbonic anhydrase (CA) it produces can effectively accelerate the hydration reaction of CO_2 to produce HCO_3^-. Under alkaline conditions, HCO_3^- reacts rapidly with OH- to generate CO_3^{2-}, which continuously forms carbonate with cations in the environment. The biochemical reactions of microbial-induced $CaCO_3$ deposition in the H_2O-CO_2-Ca^{2+} system can be represented by Eqs 1–4 (Yin, 2020):

$$CO_2 + H_2O \rightarrow HCO_3^- + H^+ \quad (1)$$

$$HCO_3^- + OH^- \rightarrow CO_3^{2-} + H_2O \quad (2)$$

$$Ca^{2+} + Cell \rightarrow Cell \sim Ca^{2+} \quad (3)$$

$$Cell \sim Ca^{2+} + CO_3^{2-} \rightarrow Cell \sim CaCO_3 \quad (4)$$

Bacillus glabrata was incubated in 400 mL of cement-simulating pore solution (Cement: water = 1:20, incubated for 30 min and sealed for 10 h) and 400 mL of deionized water. The OD600 values were determined at the corresponding time using a multifunctional enzyme marker (Varioskan LUX). As shown in Figure 2, three growth cycles existed in the two culture solvents: adjustment, growth, and stabilization periods. There were some differences in growth trends because the pH of the pore solution was higher than that of deionized water. The peak OD600 value in the stabilization period was only about 10% lower than that in the deionized water environment, indicating that microorganisms can still grow effectively in the cement pore solution.

2.1.3 Specimen preparation

Cement test blocks can be divided into four types: 1) carbonation curing specimens with added BM, denoted as BCC; 2) ordinary carbonation curing specimens, denoted as CC; 3) standard curing specimens with added BM, denoted as BSC; and 4) ordinary standard curing specimens, denoted as SC. The process of BCC preparation can be outlined as shown in Figure 3. Firstly, BM was added to water in advance and incubated with oscillation for 3 h until the spores sprouted in the solution, and the amount of BM was kept at 3% of the cement mass. Subsequently, the bacterial solution was mixed with cement instead of water to make pieces, and the water-cement ratio used was 0.5, the grey-sand ratio was 1:3, and prismatic mortar specimens with dimensions of 40 mm × 40 mm × 160 mm, and cubic net mortar specimens

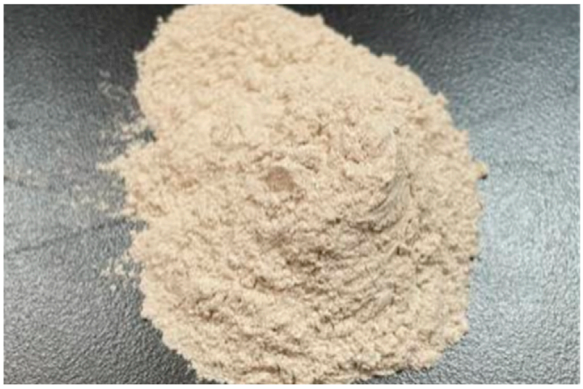

FIGURE 1
Appearance of BM.

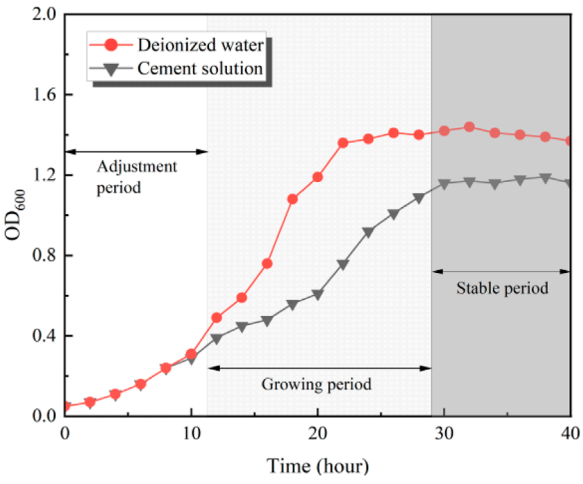

FIGURE 2
Microbial growth in simulated solutions and deionised water.

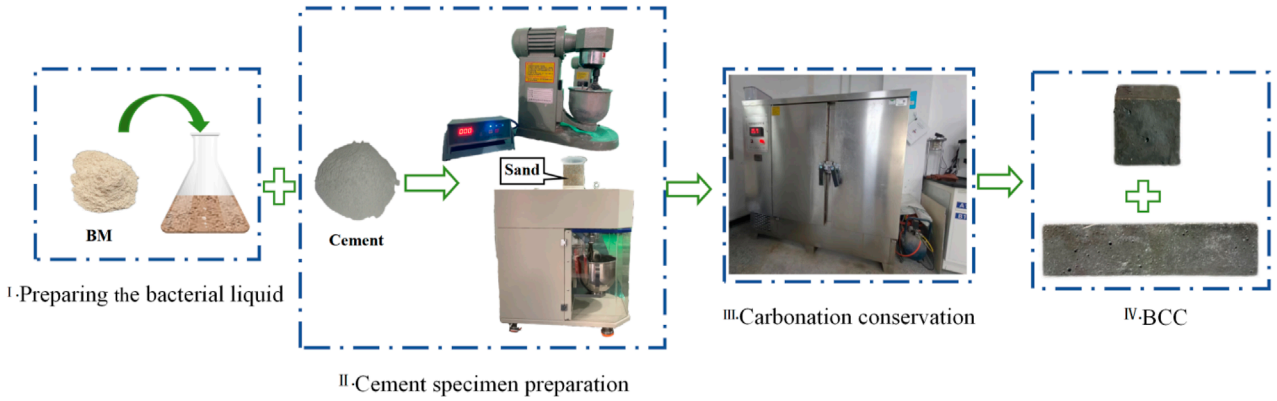

FIGURE 3
BCC preparation process.

TABLE 2 Proportion of raw materials for cement mortar specimen and cement sand specimen.

Code	Samples	Notation	Cement (g)	BM (g)	Water (g)	Sand (g)	Curing system
1	Paste (Micro and stability test)	BCC	300	9	90	0	CO_2 Curing
2		CC	300	0	90	0	
3		BSC	300	9	90	0	Standard Curing
4		SC	300	0	90	0	
5	Mortar (Strength test)	BCC	450	13.5	225	1,350	CO_2 Curing
6		CC	450	0	225	1,350	
7		BSC	450	13.5	225	1,350	Standard Curing
8		SC	450	0	225	1,350	

with dimensions of 40 mm × 40 mm × 40 mm were made. Finally, carbonation curing was carried out: the specimens were demoulded within 10 h of molding, and the molded specimens were placed in pre-conservation under moving air at a temperature of 20°C ± 2°C and a humidity of 60% ± 5% for 24 h. The pre-conserved specimens were placed in a carbonation box with a humidity of 60%–70%, a CO_2 concentration of 20%, and a carbonation curing time of 28 days. Except for the adoption of the standard curing, the steps of the preparation of the BSCs were the same as the above-mentioned types of curing. types are the same. The standard curing is to put the specimens into the standard curing room with temperature 20°C ± 1°C and relative humidity RH ≥ 95% after molding for 1 day and then molded, then numbered, and after de-molding, the specimens should be put into the saturated lime water solution at temperature 20°C ± 1°C immediately and continue to curing until 28 days. The ratios of the specimens and the curing system of BCC, CC, BSC, and SC are shown in Table 2.

2.2 Sulfate erosion

Specimen erosion method in accordance with the Chinese standard GB/T 749-2008, the maintenance of the specimen is completely immersed in a container containing 5% concentration of Na_2SO_4 solution immersed, each specimen body to add at least 200 mL of the erosion solution, the liquid surface above the top surface of the specimen of at least 10 mm, the container with a lid. Specimens in the immersion process, the ambient temperature was fixed at 5°C, once a day using sulfuric acid (1 + 5) titration of sulfate erosion solution, in order to neutralise the specimen in the solution released Ca $(OH)_2$, while titrating and stirring to keep the pH of the solution below 8.5, and monthly renewal of the solution. The specimens were taken out at the corresponding test age and dried under natural conditions for 12 h before measuring the compressive strength, expansion rate, product composition, pore structure and microscopic morphology.

2.3 Test methods

2.3.1 Degree of carbonation

Using the press to split the specimen transversely, 1% phenolphthalein alcohol solution was sprayed on the damaged surface, after about 30 s, the carbonation depth was measured at one measurement point every 10 mm (3 specimens per group, a total of 18 measurements points for each specimen), and the average value was taken as the carbonation depth of the specimen, which was measured to an accuracy of 0.1 mm. The carbonation rate is the ratio of the amount of CO_2 consumed in the carbonation maintenance reaction to the theoretical maximum amount of CO_2 consumed. Adopt the burning weight loss method to determine the degree of carbonation maintenance of the net pulp specimens, two net pulp specimens as a group of 1, with a pulveriser to the specimens into powder, and through the blender to mix the powder, take (10 ± 1) g of powder for the test. Before being burned in the high-temperature furnace, the powder was dried in a vacuum oven at (60 ± 2) °C until the mass was constant. Then, the purified powder was put into a high-temperature furnace and heated to 500°C and 950°C, respectively, to quantify the content of calcium carbonate in the product. The reaction equations are as follows (5, 6) (Zhan et al., 2013):

$$\alpha = (m_{500°C} - m_{950°C})/(m_c \times M_{max}) \times 100\% \quad (5)$$

$$M_{max} = 0.785(m_{CaO} - 0.7SO_3) + 1.09MgO + 1.42Na_2O + 0.93K_2O \quad (6)$$

Where: α is the carbonation rate of the net paste specimen; $m_{500°C}$ is the mass of the net paste specimen after burning at 500°C; $m_{500°C}$ is the mass of the net paste specimen after burning at 950°C; m_c is the mass of the net paste specimen; M_{max} is the theoretical maximum degree of carbonation preservation of the net paste specimen CaO, SO_3, MgO, Na_2O and K_2O is the content of oxides in the cement clinker.

2.3.2 Mechanical property

The compressive strength of mortar specimens after 0, 30, 60, 90, 120, and 180 days of immersion were tested according to the Chinese standard GB/T17671-2021 and the average compressive strength of six samples was recorded as the final result.

2.3.3 Expansion rate test

The expansion rate test was conducted according to the Chinese standard GB/T 749-2008, where the initial length of the 28-day standard maintenance samples was measured by a length comparator prior to immersion, and the change in length was measured after 15, 30, 60, 90, 120, and 180 days of immersion, and the average of the three samples was recorded.

2.3.4 Composition of products

The crystalline phases in the samples before and after erosion were quantified by XRD using CuKα radiation (λ = 0.15419 mm) with a 2θ range of 5°–70° and a scan rate of 0.02 (°)/s, and the composition of the physical phases was quantified by Rietveld refinement. Twenty percent TiO2 was added to each sample as an internal standard. For net paste sampling, a superficial 2 mm layer of net paste powder was taken and placed in anhydrous ethanol (7 days) to stop hydration, after which the powder was dried in a vacuum oven at 60°C for 72 h to completely dry the powder, and then the dried samples were ground and sieved through a 0.045 mm sieve for XRD testing.

FIGURE 4
Photographs of cemented sand specimens after curing.

2.3.5 Hole structure analysis

A precision cutter was used to cut down the samples of 2 mm from the surface layer of the eroded surface, saturated with water, and then LF-NMR was used to measure the changes in the pore structure of the mortar specimens, and to study the changes in the distribution of different pore sizes of the pore structure of the surface mortar specimens under sulfate erosion.

2.3.6 Microcosm

The micro-morphology was observed by SEM, the net pulp specimens were taken and cut perpendicular to the erosion surface with a precision cutter, and the flat samples of the net pulp pieces were placed in a vacuum drying oven at 60°C for 72 h, so as to make the pieces of the net pulp completely dry, and the dried pieces of the net pulp were placed in a nail-shaped sample stage for spraying of the gold, and then the SEM was used to study the change of micro-morphology of the carbon-conditioned products under sulfate erosion.

3 Results and discussion

3.1 Degree of carbonation

As can be seen from Figures 4, 5, for the normal curing specimens, the carbonation rate of the specimens after adding BM increased from 6.11% to 9.72%, compared with the carbonation rate of the control group increased by 59.08%; for the carbonation curing specimens after adding BM, the carbonation rate of the specimens increased from 43.12% to 72.43%, compared with the control group carbonation rate increased by 67.97%; the carbonation depths of the four specimens, namely, SC, BSC, CC and BCC, were 0.1.7, 8.8 and 13.3 mm, respectively. The carbonation depths of SC, BSC, CC, and BCC were 0, 1.7, 8.8, and 13.3 mm, respectively, and the carbonation depths and carbonation rates of the four specimens were generally similar. It can be seen that the addition of BM effectively accelerated the carbonation process of cement specimens in both carbonation and standard curing, and the cement specimens achieved a better carbonation effect under the dual effect of carbonation curing and mineralized bacteria.

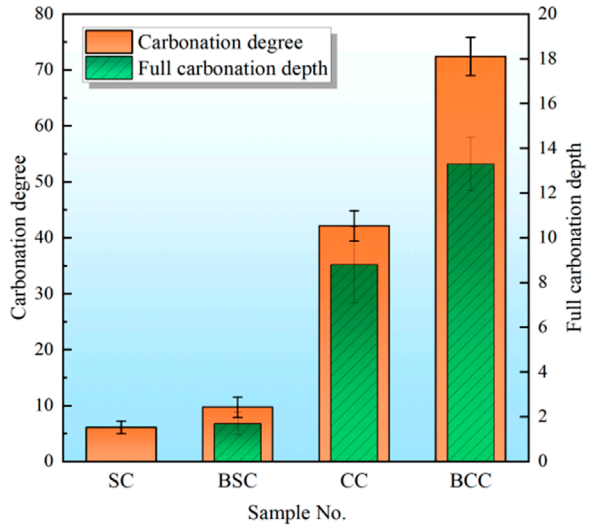

FIGURE 5
Full carbonation degree and Carbonation degree of cement sand specimens.

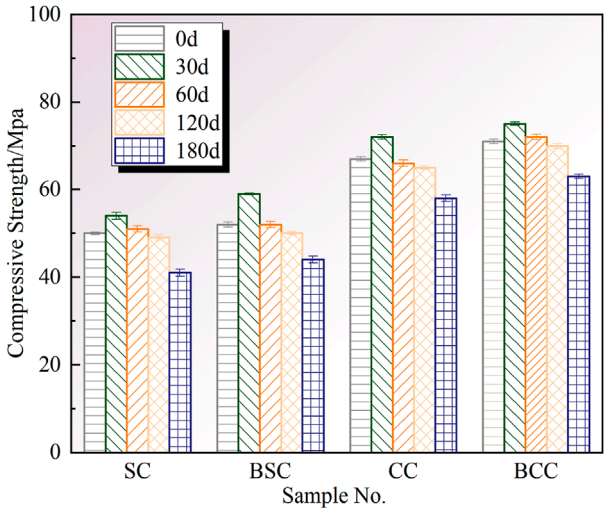

FIGURE 6
Compressive strength of cemented sand specimens after sulfate attack.

3.2 Compressive strengths

The changes in compressive strength of mortar specimens at different erosion ages are shown in Figure 6, which shows that both carbonation curing and standard curing doped with mineralizing bacteria can effectively improve the initial compressive strength of specimens, and the BCC and BSC initial test compressive strengths were 71 and 52 MPa, respectively, which were 5.97% and 4.00% higher than that of the control specimens, indicating that under the condition of carbonation curing, the enhancement effect of mineralizing bacteria was is more obvious. The compressive strength of all specimens increased after 30 days of immersion in sulfate solution and then decreased with the prolongation of erosion time, specifically, the compressive strength of all specimens increased by 5.94%–11.54% after 30 days of immersion. After 60 days of erosion, the compressive strength of the specimens decreased to the level before immersion. After 180 days of erosion, the compressive strengths of BCC, CC, BSC, and SC specimens were 63, 58, 44, and 41 MPa, respectively, which were 11.27, 13.43, 15.38, and 18.00% lower than the strengths before erosion, respectively. The loss of compressive strengths of the experimental group doped with mineralized bacteria was lower than that of the control group, this is attributed to the fact that the mineralised $CaCO_3$ fills the pores of the cement matrix, which reduces the water absorption of the specimen and improves the permeability. (Chen et al., 2021). The smallest percentage of strength loss was observed in BCC, which indicates that the synergistic effect of biomineralization and carbonation maintenance significantly improved the resistance of cementitious materials to sulfate erosion.

3.3 Expansion rate

Figure 7 demonstrates the expansion of cementitious sand specimens with different times of sulfate attack. It can be clearly seen that by the erosion effect of sulfate solution, there are specimens have different degrees of volume expansion. After a month of erosion, the volumetric expansion of the specimens first showed a rapid increase, followed by a slow increase in expansion with increasing time of sulfate erosion. Microbial mineralization inhibited the volume expansion of the cement specimens, and after 180 days of sulfate erosion, the BCC and BSC expansion rates were reduced by 5.97% and 4.00%, respectively, compared to the control specimens. Mineralizing bacteria may enhance the erosion resistance of cementitious sand specimens by producing substances such as calcium carbonate (Khushnood et al., 2020). Therefore, the use of carbon-conditioned cementitious materials doped with mineralizing bacteria may be considered to improve the durability of structures in sulfate erosion environments.

3.4 Composition of products

The physical phases of the net paste specimens before and after immersion in sodium sulfate solution were analyzed qualitatively and quantitatively by XRD tests, and the results are shown in Figure 8. As can be seen from Figure 8A, tricalcium silicate (C_3S), dicalcium silicate (C_2S), calcium hydroxide (CH), and calcium carbonate ($CaCO_3$) can be observed in the specimens before immersion. Among them, in the two groups of specimens with standard maintenance, it can be observed that $Ca(OH)_2$ still has a high content, indicating that a large amount of unreacted $Ca(OH)_2$ exists in the two systems; while a large amount of $CaCO_3$ exists in CC and BCC, indicating that the carbonation maintenance accelerated the rate of the carbonation reaction of the cementitious materials, and only a trace amount of $Ca(OH)_2$ exists in BCC, and the system $Ca(OH)_2$ has been fully reacted. From the content of $CaCO_3$, it can be seen that the mineralization of microorganisms significantly increased the generation of calcium carbonate in the system, and the carbonic anhydrase generated by microorganisms, which accelerates the rate of water and reaction of carbon dioxide

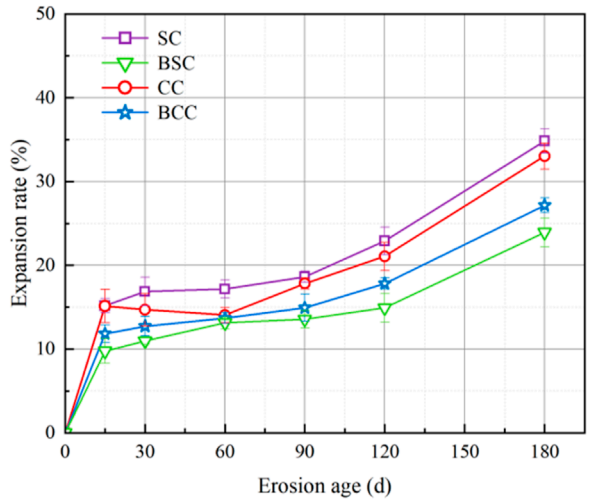

FIGURE 7
Length deformation of cemented sand specimens after sulfate attack.

and increases the content of carbonate in the reaction system and accelerates the rate of calcium carbonate generation (Singh and Gupta, 2020), which is consistent with the results of the analysis of the degree of carbonation. Due to the continued hydration of C_3S and C_2S in the pre-immersion period caused by as well as the erosion of C_3S, C_2S, CH by sulfate, the generation of $CaCO_3$ and indeterminate silica gel, BCC, CC, BSC specimens ofC_3S, C_2S, and CH in the immersion of the 15 days after the basic reaction is complete (Figure 8B). In the pre-immersion period, although the $CaCO_3$ in the surface layer was directly dissolved and decalcified under sulfate erosion, the erosion reaction rate of C_3S, C_2S, and CH was faster, and the generated $CaCO_3$ and indeterminate silica gel filled the pores of the specimens, which was the main reason for the increase in compressive strength of the specimens after 15 days of immersion. In addition, with the increase of erosion time, the diffraction peak intensity of CaCO3 in the net slurry was first enhanced and then decreased, and the CaCO3 content began to decrease after 30 days of immersion, which was attributed to the fact that the surface layer of the specimen, C_3S, C_2S and CH were eroded by the sulfate solution (Figures 8C–F), and the surface layer of the $CaCO_3$ continued to be eroded, generating the soluble $Ca(HCO_3)_2$, which led to the dissolution of calcium, which was the main reason for the first rise of the specimen compressive strength and then decreased, and this stage of the test piece was the main reason for the rise of the compressive strength. increases and then decreases, and this stage is also accompanied by the decalcification of the C-S-H gel (Rimmelé et al., 2008; Yang, 2023). In Figure 8F, it can be found that the $CaCO_3$contents of the carbonation maintenance groups were all higher than those of the control group after 180 days of immersion, indicating that the carbonation maintenance can reduce the dissolution of calcium ions from cementitious materials in sulfate attack, and the addition of mineralizing bacteria improves the effect of the cementitious materials in the resistance to sulfate attack. The corrosion products of $CaCO_3$ in the CC, CC, and BSC were mainly calcite and aragonite-based, and those in the SC were mainly calcite and spherulitic aragonite predominated.

3.5 Hole structure analysis

The pore structure distribution of the mortar specimens before and after the sulfate attack is shown in Figure 9. It can be observed that microbial mineralization can reduce the porosity of the specimens. This is because biomineralisation forms a dense $CaCO_3$ precipitate layer on the surface of the cement specimen, which fills the pores of the cement matrix, resulting in a denser structure of the cementitious material and refinement of the pore size. (Seifan and Ebrahiminezhad, 2019). The pores in cement-based materials can be divided into gel nanopores (<10 nm), fine capillary pores (10–50 nm), medium capillary pores (50–100 nm), large capillary tube pores (100–5,000 nm), and macropores (>5,000 nm) according to their size (Liu et al., 2019). According to Figure 9, it can be found that the mineralization effect on the refinement of cement-based materials is concentrated in large capillary tube pores and macropores, reducing the number of large capillary tube pores and macropores, increasing the number of fine and medium capillary pores, and improving the impermeability and durability of the specimens (Feng et al., 2021). The porosity of the mortar specimens shows an upward trend with the increase of erosion time. After 180 days of erosion, the porosity of BCC, CC, BSC, and SC is 14.52%, 16.54%, 17.26%, and 19.15% respectively. The biological specimen has a porosity reduction of 9.87–12.21% compared with its control group, indicating that MICP technology can effectively improve the sulfate resistance of cement-based materials. The proportion of gel pores and fine capillary pores below 50 nm increases first and then decreases with the increase of erosion time, while the proportion of medium capillary pores, large capillary tube pores, and macropores above 50 nm decreases first and then increases. XRD analysis results show that this is because in the early stage of immersion, the corrosion products $CaCO_3$ and amorphous silica filled the pores, and as the sulfate attack worsened, the content of gypsum and calcium aluminate increased, which deteriorated the pore structure of the specimens, increased the porosity, led to the decrease of the strength of the specimens, and began to peel off the surface layer (Qin et al., 2021).

3.6 Microcosm

Figure 10 shows the micro-morphology of different samples before and after erosion. Before erosion, a large amount of plate-like $Ca(OH)_2$ existed in the SC specimen (Figure 8A), while a large amount of prismatic $CaCO_3$ appeared in the BSC, CC, and BCC matrix, and $CaCO_3$ encapsulated the C-S-H gel and other hydration products and formed a dense layer of calcium carbonate in the surface layer of the C-S-H gel. Based on this morphology combined with XRD analysis and literature, it can be deduced that this crystal type in the carbonated cement specimen is calcite; the microbial specimens produced smaller and uniformly distributed $CaCO_3$ crystals, thus optimizing the internal microstructure of the cement specimens, which positively affected the resistance of the specimens to sulfate attack. Figure 10D demonstrates that more microscopic pores were generated inside the SC specimens after 180 days of erosion, which was due to the looser $CaCO_3$ formed after $Ca(OH)_2$ erosion, and the looser structure of the specimens, which resulted in more microcracks, leading to a faster diffusion rate of the

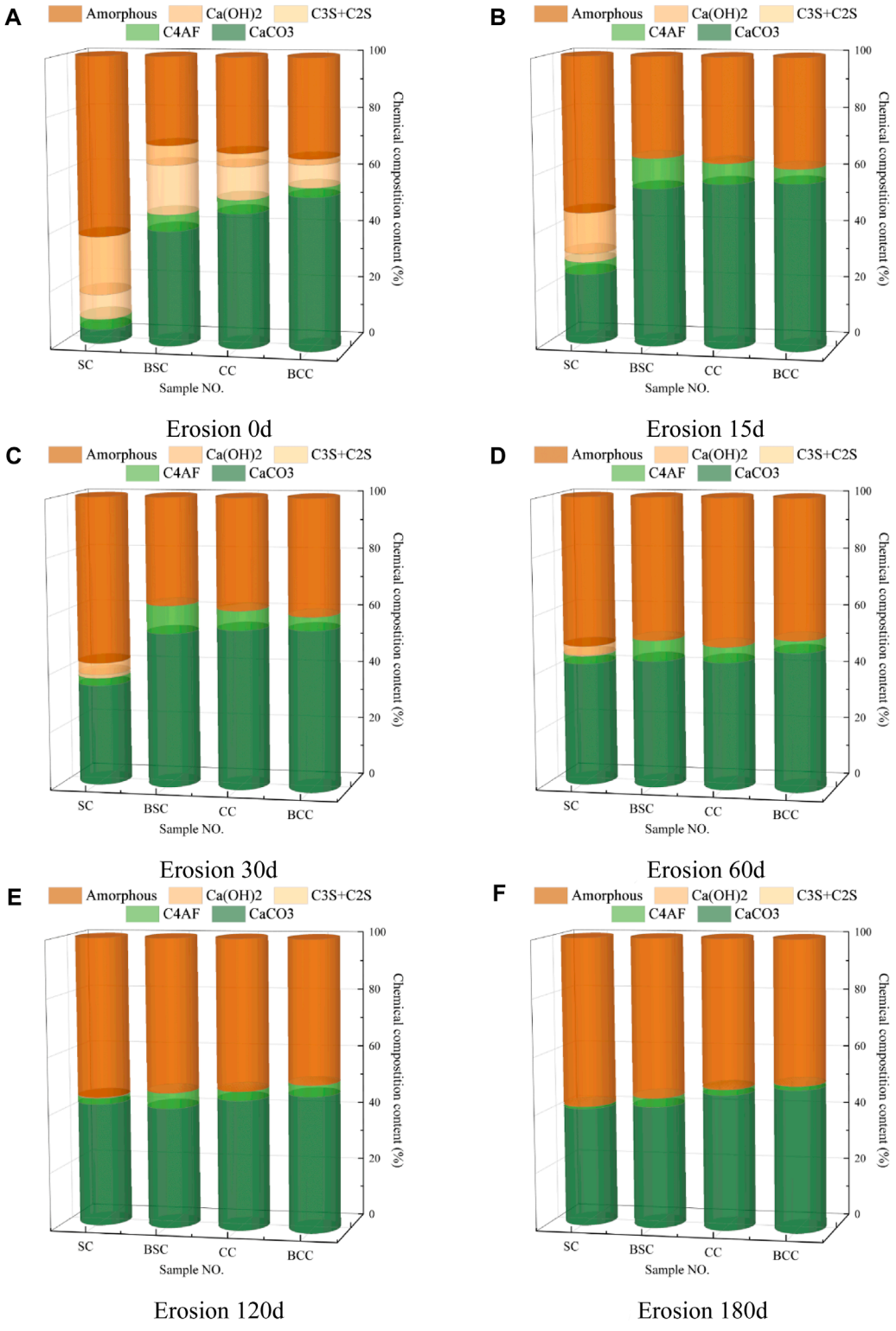

FIGURE 8
Content of each physical phase of the net mortar specimens after sulfate erosion. **(A)** Erosion 0d, **(B)** Erosion 15d, **(C)** Erosion 30d, **(D)** Erosion 60d, **(E)** Erosion 120d, **(F)** Erosion 180d.

sulfate solution into the interior, which led to a further deepening of the erosion effect. It can be seen that the cellular voids of microbial specimens are less than those of the control group, which is because the cell wall of the bacteria has a negative charge, and the positively charged Ca^{2+} is adsorbed on the surface of the cell and combined with CO_3^{2-} to generate $CaCO_3$, which contains a large amount of

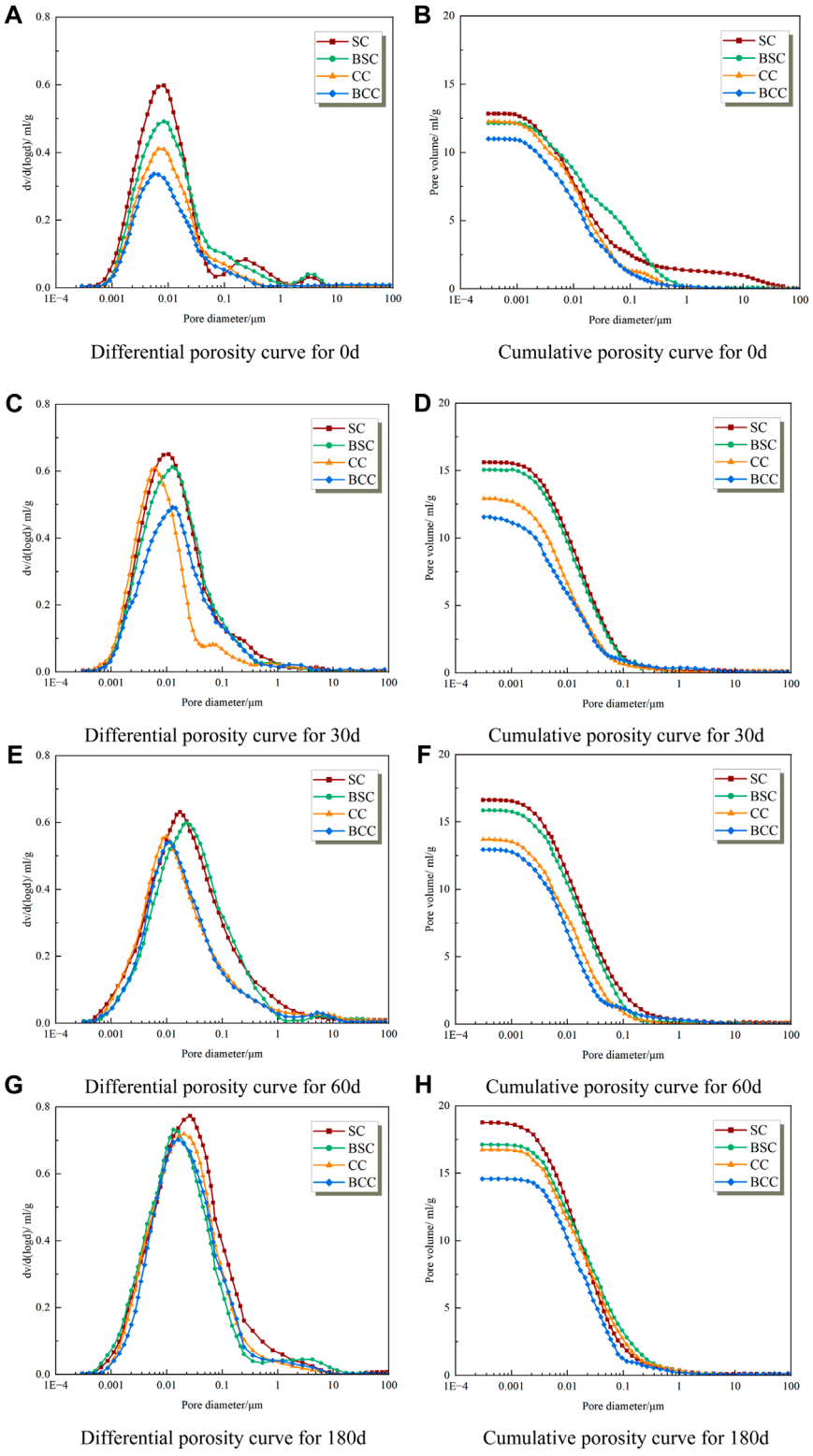

FIGURE 9
Pore structure change of mortar specimen after sulfate attack. **(A)** Differential porosity curve for 0d, **(B)** Cumulative porosity curve for 0d, **(C)** Differential porosity curve for 30d, **(D)** Cumulative porosity curve for 30d, **(E)** Differential porosity curve for 60d, **(F)** Cumulative porosity curve for 60d, **(G)** Differential porosity curve for 180d, **(H)** Cumulative porosity curve for 180d.

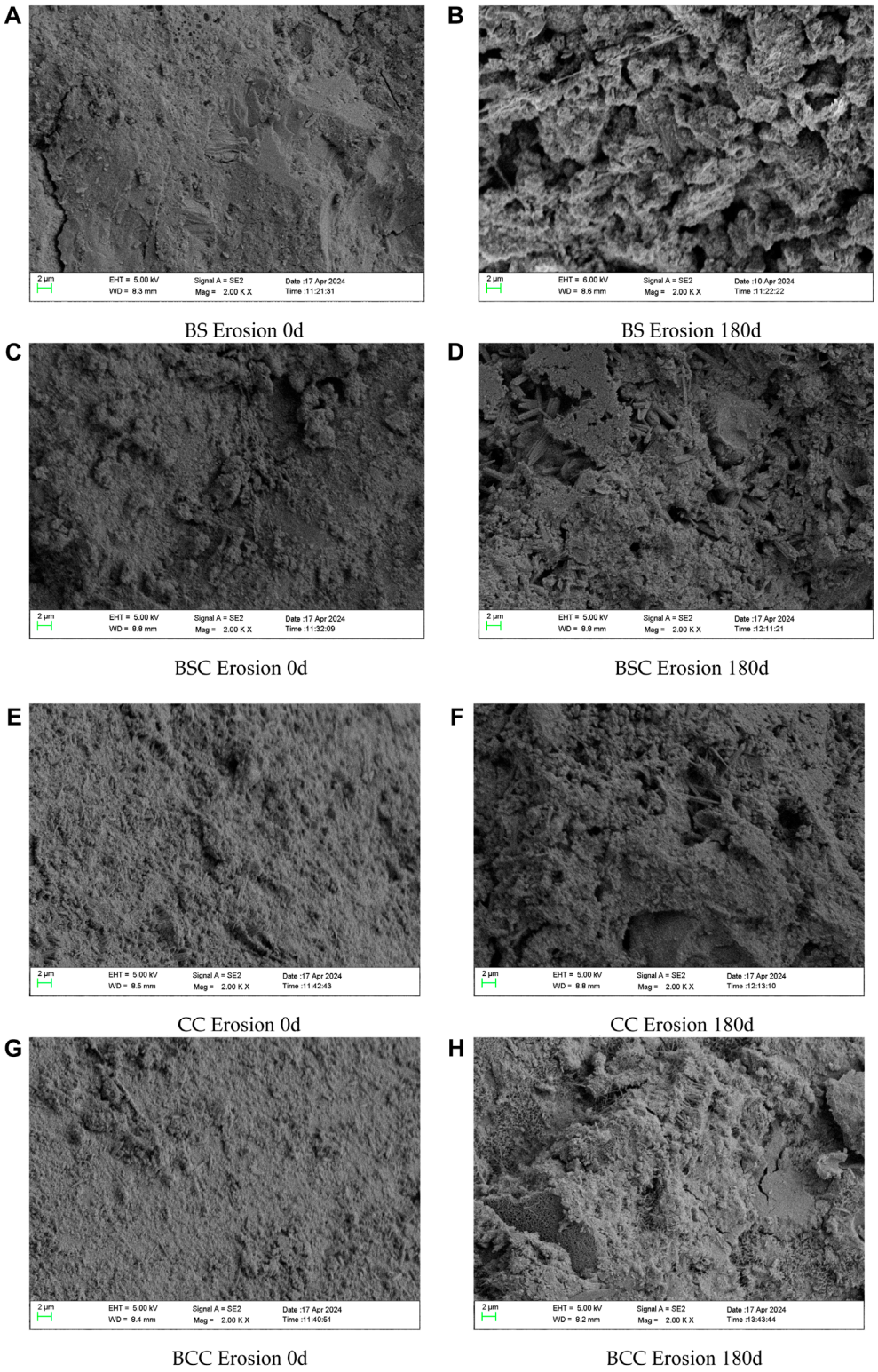

FIGURE 10
SEM imaging of cement specimens before and after immersion. **(A)** BS Erosion 0d, **(B)** BS Erosion 180d, **(C)** BSC Erosion 0d, **(D)** BSC Erosion 180d, **(E)** CC Erosion 0d, **(F)** CC Erosion 180d, **(G)** BCC Erosion 0d, **(H)** BCC Erosion 180d.

calcite, which has a slower dissolution rate than $Ca(OH)_2$, and at the same time, the presence of the $CaCO_3$ layer plugs the surface pore defects of the specimen and improves the erosion effect. At the same time, the presence of the $CaCO_3$ layer blocked the surface pore defects of the specimen and improved the impermeability, thus blocking the transport path of sulfate ions and improving

the sulfate erosion resistance of the specimen. After 180 days of erosion, the microscopic morphology of the BCC did not find obvious microcracks, but the BSC still had more pores, indicating that the microorganisms have limited improvement of the sulfate erosion resistance of the cementitious materials under the standard curing conditions and that the combination of the carbonation curing can effectively improve the sulfate erosion resistance of the cementitious materials. sulfate erosion resistance of cementitious materials.

4 Conclusion

This study investigates the impact of MICP technology on the long-term durability of cement-based materials subjected to sulfate attack. The effect of incorporating BM on the mechanical strength and volumetric expansion of cement specimens cured under carbonation and standard conditions after soaking in sulfate solutions for various durations was examined. Additionally, XRD/Rietveld, LF-NMR, and SEM tests were utilized to reveal the mechanism by which microbial mineralization resists sulfate erosion. Based on the experimental results above, the following conclusions can be drawn:

1) All specimens showed a trend of increasing and then decreasing compressive strength during the erosion of sulphate solution, and the compressive strength of the glued sand specimens decreased by 11.27%–18.00% after 180 days of immersion in sulphate solution, and the BM could reduce the strength loss by 14.53%–16.12%.
2) The volumetric expansion of the glued sand specimens increased with the prolongation of the immersion time in the sulphate solution, and this expansion could be suppressed by the addition of BM, and the BCC and BSC expansions were reduced by 5.97% and 4.00%, respectively, compared to the control specimens.
3) The results of XRD and microscopic void analyses show that microbial mineralised calcite improves the densification of the specimens by improving the pore structure, thus hindering the inward diffusion rate of sulphate solution and increasing the resistance of cementitious materials to the erosion of sulphate solution.
4) SEM images confirm that microbial mineralisation promotes the formation of more homogeneous, fine CaCO3 crystals that fill the voids between the C-S-H gel and other hydration products, thereby significantly enhancing the microstructure and durability of the cementitious materials.
5) This study verified that the MICP technique can improve the early resistance of cementitious materials to sulphate erosion, but the understanding of the microstructural changes and erosion mechanism of the materials after microbial mineralisation is not comprehensive enough, especially the comparative analysis of the material performance under different maintenance conditions is not clear. Therefore, future studies should consider longer time scale erosion tests to explore the effects of multiple microorganisms on the performance of cementitious materials and analyse the erosion mechanism and durability performance in depth to obtain a more comprehensive understanding.

Data availability statement

The original contributions presented in the study are included in the article/Supplementary Material, further inquiries can be directed to the corresponding author.

Author contributions

YZ: Writing–review and editing, Writing–original draft, Funding acquisition, Conceptualization. GP: Writing–original draft. AL: Writing–original draft, Visualization. XY: Writing–review and editing, Supervision. SK: Writing–original draft, Investigation. YA: Writing–original draft, Formal Analysis. JT: Writing–original draft, Formal Analysis. XS: Writing–review and editing, Writing–original draft, Validation.

Funding

The author(s) declare that financial support was received for the research, authorship, and/or publication of this article. This study is supported by the National Key R&D Program of China (2022YFB2601900), National Natural Science Foundation of China, (Nos 51208287 and U2233210), the Beijing Scholars Foundation (No. 067) and the Natural Science Foundation of Shandong Province (NO. ZR2016EEM42).

Conflict of interest

Authors YZ, AL, and SK were employed by Beijing Capital International Airport Co. Authors GP and XY were employed by Beijing Municipal Road and Bridge Technology Development Co.

The remaining authors declare that the research was conducted in the absence of any commercial or financial relationships that could be construed as a potential conflict of interest.

Publisher's note

References

Ahmad, M. A., Liu, B., Li, Q. W., Adeel, M., Zhang, J., Zhou, Y., et al. (2023). Bio-deposition approaches for sustainable execution of recycled aggregates in concretes. *Front. Mater.* 10, 1131673. doi:10.3389/FMATS.2023.1131673

Chaurasia, L., Bisht, V., Singh, L., and Gupta, S. (2019). A novel approach of biomineralization for improving micro and macro-properties of concrete. *Constr. Build. Mater.* 195, 340–351. doi:10.1016/j.conbuildmat.2018.11.031

Chen, Y. F. (2020). "Carbonation curing mechanism of cement-based materials and its improvement on pervious concrete,". Doctor's Thesis (Harbin, China: Harbin Institute of Technology).

Chen, Y. Q., Qian, C. X., Hao, Z. X., and Zhou, H. (2021). Effect of bio-mineralization on concrete performance: carbonation, microhardness, gas permeability and Cl-migration. *Biochem. Eng. J.* 171, 108024. doi:10.1016/J.BEJ.2021.108024

Ding, Z. Z., Quy, N. X., Noguchi, T., Kim, J., and Hama, Y. (2022). A study on the change in frost resistance and pore structure of concrete containing blast furnace slag under the carbonation conditions. *Constr. Build. Mater.* 331, 127295. doi:10.1016/j.conbuildmat.2022.127295

Dixit, A., Du, H. J., and Pang, S. D. (2021). Carbon capture in ultra-high performance concrete using pressurized CO2 curing. *Constr. Build. Mater.* 288, 123076. doi:10.1016/J.CONBUILDMAT.2021.123076

Falchetto, A. C., Moon, K. H., Wang, D., and Riccardi, C. (2018). Investigation on the cooling medium effect in the characterization of asphalt binder with the bending beam rheometer (BBR). *Can. J. Civ. Eng.* 45, 594–604. doi:10.1139/cjce-2017-0586

Feng, J., Chen, B. C., Sun, W. W., and Wang, Y. (2021). Microbial induced calcium carbonate precipitation study using Bacillus subtilis with application to self-healing concrete preparation and characterization. *Constr. Build. Mater.* 280, 122460. doi:10.1016/J.CONBUILDMAT.2021.122460

Jia, X. X. (2020). "Effect of accelerated carbonation curing on the properties and microstructure of hardened cement paste,". Master's Thesis (Hunan, China: Hunan University).

Jiang, C. M., Lin, Y., Tang, X. J., Chu, H., and Jiang, L. (2021). Deterioration process of high belite cement paste exposed to sulfate attack, calcium leaching and the dual actions. *J. Mater. Res. Technol.* 15, 2982–2992. doi:10.1016/J.JMRT.2021.09.125

Kashef-Haghighi, S., Shao, Y. X., and Ghoshal, S. (2015). Mathematical modeling of CO 2 uptake by concrete during accelerated carbonation curing. *Cem. Concr. Res.* 67, 1–10. doi:10.1016/j.cemconres.2014.07.020

Khushnood, A. R., Qureshi, A. Z., Shaheen, N., and Ali, S. (2020). Bio-mineralized self-healing recycled aggregate concrete for sustainable infrastructure. *Sci. Total Environ.* 703, 135007. doi:10.1016/j.scitotenv.2019.135007

Li, M. L., and Gan, F. (2023). Experimental study of high temperature on the shear properties of early-age concrete. *Front. Mater.* 10, 1280057. doi:10.3389/FMATS.2023.1280057

Liang, C. F., Pan, B. H., Ma, Z. M., He, Z. H., and Duan, Z. H. (2020). Utilization of CO 2 curing to enhance the properties of recycled aggregate and prepared concrete: a review. *Cem. Concr. Comp.* 105, 103446. doi:10.1016/j.cemconcomp.2019.103446

Liang, H. X., Liu, Y. Q., Tian, B. H., Li, Z., and Ou, H. (2022). A sustainable production of biocement via microbially induced calcium carbonate precipitation. *Int. Biodeterior. Biodegr.* 172, 105422. doi:10.1016/J.IBIOD.2022.105422

Lily, D. P., Emiliano, P., Marjan, T., David, H., Wang, D., Mikhailenko, P., et al. (2022). RILEM interlaboratory study on the mechanical properties of asphalt mixtures modified with polyethylene waste. *J. Clean. Prod.* 375, 134124. doi:10.1016/j.jclepro.2022.134124

Liu, J. H., Shi, C. J., Farzadnia, N., and Ma, X. W. (2019). Effects of pretreated fine lightweight aggregate on shrinkage and pore structure of ultra-high strength concrete. *Constr. Build. Mater.* 204, 276–287. doi:10.1016/j.conbuildmat.2019.01.205

Meng, Y. Z., Ling, T. C., Mo, K. H., and Tian, W. H. (2019). Enhancement of high temperature performance of cement blocks via CO2 curing. *Sci. Total. Environ.* 671, 827–837. doi:10.1016/j.scitotenv.2019.03.411

Osman, K. M., Taher, F. M., Abd El-Tawab, A., and Faried, A. S. (2021). Role of different microorganisms on the mechanical characteristics, self-healing efficiency, and corrosion protection of concrete under different curing conditions. *J. Build. Eng.* 41, 102414. doi:10.1016/J.JOBE.2021.102414

Polettini, A., Pomi, R., and Stramazzo, A. (2016). CO 2 sequestration through aqueous accelerated carbonation of BOF slag: a factorial study of parameters effects. *J. Environ. Manage.* 167, 185–195. doi:10.1016/j.jenvman.2015.11.042

Qin, L., Gao, X. J., Su, A. S., and Li, Q. (2021). Effect of carbonation curing on sulfate resistance of cement-coal gangue paste. *J. Clean. Prod.* 278, 123897. doi:10.1016/j.jclepro.2020.123897

Qin, L., Mao, X. T., Gao, X. J., Zhang, P., Chen, T., Li, Q., et al. (2022). Performance degradation of CO2 cured cement-coal gangue pastes with low-temperature sulfate solution immersion. *Case Stud. Const. Mat.* 17, e01199. doi:10.1016/J.CSCM.2022.E01199

Rimmelé, G., Barlet-Gouédard, V., Porcherie, O., Goffé, B., and Brunet, F. (2008). Heterogeneous porosity distribution in Portland cement exposed to CO 2 -rich fluids. *Cem. Concr. Res.* 38, 1038–1048. doi:10.1016/j.cemconres.2008.03.022

Rostami, V., Shao, Y. X., and Boyd, A. J. (2012). Carbonation curing versus steam curing for precast concrete production. *J. Mater. Civ. Eng.* 24, 1221–1229. doi:10.1061/(ASCE)MT.1943-5533.0000462

Rui, Y. F., and Qian, C. X. (2022). The influence of bacteria on biologically induced calcium carbonate and its evolution process. *J. Cryst. Growth.* 581, 126515. doi:10.1016/J.JCRYSGRO.2022.126515

Salvatore, V. (2021). Effect of different environments' conditioning on the debonding phenomenon in fiber-reinforced cementitious matrix-concrete joints. *Materials* 14, 7566. doi:10.3390/ma14247566

Santhanam, M., Cohen, D. M., and Olel, J. (2003). Effects of gypsum formation on the performance of cement mortars during external sulfate attack. *Cem. Concr. Res.* 33, 325–332. doi:10.1016/S0008-8846(02)00955-9

Seifan, M., Ebrahiminezhad, A., Ghasemi, Y., and Berenjian, A. (2019). Microbial calcium carbonate precipitation with high affinity to fill the concrete pore space: nanobiotechnological approach. *Bioprocess. Biosyst. Eng.* 42, 37–46. doi:10.1007/s00449-018-2011-3

Seo, J. H., Park, S. M., and Lee, H. K. (2018). Evolution of the binder gel in carbonation-cured Portland cement in an acidic medium. *Cem. Concr. Res.* 109, 81–89. doi:10.1016/j.cemconres.2018.03.014

Sha, A. M., Jiang, W., Shan, J. H., Wu, W. J., Li, Y., and Zhang, S. (2022). Pavement structure and materials design for sea-crossing bridges and tunnel: case study of the Hong Kong–Zhuhai–Macau Bridge. *J. Road. Eng.* 2, 99–113. doi:10.1016/j.jreng.2022.05.002

Singh, H., and Gupta, R. (2020). Cellulose fiber as bacteria-carrier in mortar: self-healing quantification using UPV. *J. Build. Eng.* 28, 101090. doi:10.1016/j.jobe.2019.101090

Su, A. S., Chen, T. F., Gao, X. J., Li, Q. Y., and Qin, L. (2022). Effect of carbonation curing on durability of cement mortar incorporating carbonated fly ash subjected to Freeze-Thaw and sulfate attack. *Constr. Build. Mater.* 341, 127920. doi:10.1016/J.CONBUILDMAT.2022.127920

Tayebani, B., and Mostofinejad, D. (2019). Penetrability, corrosion potential, and electrical resistivity of bacterial concrete. *J. Mater. Civ. Eng.* 31, 04019002. doi:10.1061/(ASCE)MT.1943-5533.0002618

Wu, H. X., Liang, C. F., Xiao, J. Z., and Ma, Z. M. (2021). Properties and CO2-curing enhancement of cement-based materials containing various sources of waste hardened cement paste powder. *J. Build. Eng.* 44, 102677. doi:10.1016/J.JOBE.2021.102677

Wu, W. J., Cavalli, M. C., Jiang, W., and Kringos, N. (2024a). Differing perspectives on the use of high-content SBS polymer-modified bitumen. *Constr. Build. Mater.* 411, 134433. doi:10.1016/j.conbuildmat.2023.134433

Wu, W. J., Jiang, W., Xiao, J. J., Yuan, D. D., Wang, T., and Ling, X. W. (2024b). Investigation of LAS-based fatigue evaluation methods for high-viscosity modified asphalt binders with high-content polymers. *Constr. Build. Mater.* 422, 135810. doi:10.1016/j.conbuildmat.2024.135810

Xian, X. P., Zhang, D., Lin, H., and Shao, Y. X. (2022). Ambient pressure carbonation curing of reinforced concrete for CO2 utilization and corrosion resistance. *J. CO2. Util.* 56, 101861. doi:10.1016/j.jcou.2021.101861

Xing, W., Zhou, F., Zhu, R., Wang, X. D., and Chen, T. Z. (2023). Performance and mechanism of Zn-contaminated soil through microbe-induced calcium carbonate precipitation. *Buildings* 13, 1974. doi:10.3390/buildings13081974

Xu, W. B., Hou, Z. K., Yang, W., Chen, Q., Liu, H., Feng, S., et al. (2024). *In-situ* detection method of water content in newly poured concrete. *J. Intell. Constr.* 2, 9180033. doi:10.26599/JIC.2024.9180033

Yang, Y. (2023). "Study on sulfate corrosion resistance of SACOPC composite cement-based repair system,". Master's Thesis (Shaanxi, China: Xi'an University of Architecture and Technology).

Yin, G. J., Zuo, X. B., Sun, X. H., and Tang, Y. J. (2019). Macro-microscopically numerical analysis on expansion response of hardened cement paste under external sulfate attack. *Constr. Build. Mater.* 207, 600–615. doi:10.1016/j.conbuildmat.2019.02.159

Yin, H. H. (2020). "Effect and mechanism of microorganism on volume stability and utilization efficiency of steel slag,". Doctor's Thesis (Nanjing, China: Southeast University).

Zhan, B. S., Poon, C., and Shi, C. J. (2013). CO 2 curing for improving the properties of concrete blocks containing recycled aggregates. *Cem. Concr. Comp.* 42, 1–8. doi:10.1016/j.cemconcomp.2013.04.013

Zhang, D., Ghouleh, Z., and Shao, Y. X. (2017). Review on carbonation curing of cement-based materials. *J. CO2. Util.* 21, 119–131. doi:10.1016/j.jcou.2017.07.003

Zhang, G. Z., Wu, C., Hou, D. S., Yang, J., Sun, D., and Zhang, X. (2021). Effect of environmental pH values on phase composition and microstructure of Portland cement paste under sulfate attack. *Compos. Part B-Eng.* 216, 108862. doi:10.1016/J.COMPOSITESB.2021.108862

Zhang, S. P., Ghouleh, Z., Azar, A., and Shao, Y. X. (2021). Improving concrete resistance to low temperature sulfate attack through carbonation curing. *Mater. Struct.* 54, 37. doi:10.1617/S11527-021-01626-9

Zhang, X., Qian, C. X., Ma, Z. Y., and Li, F. (2022). Study on preparation of supplementary cementitious material using microbial CO2 fixation of steel slag powder. *Constr. Build. Mater.* 326, 126864. doi:10.1016/J.CONBUILDMAT.2022.126864